Lithuanian Journal of Physics, Vol. **52**, No. 2, pp. 126–141 (2012)

QUASI-BOUND STATES OF DIRAC ELECTRONS IN ELECTRIC AND MAGNETIC QUANTUM DOTS

A. Matulis

Semiconductor Physics Institute, Center for Physical Sciences and Technology, A. Goštauto 11, LT-01108 Vilnius, Lithuania
E-mail: amatulis@takas.lt

Received 19 March 2012; accepted 7 June 2012

The problem of quasi-bound states for ultra-relativistic Dirac electrons and holes in electric and magnetic quantum dots in graphene is discussed. It is shown that these states with a rather long lifetime appear in an electric quantum dot in the case of a large orbital momentum, and in a magnetic quantum dot if its dimensions exceed the Larmor radius of the electron. The quasi-bound state properties are analysed by using the local density of states technique the application of which is demonstrated by a simple one-dimensional model of the decaying state. In addition, the analogy between two-dimensional graphene and one-dimensional polymers is discussed, which helps in understanding and interpreting the sophisticated features of the electron spectrum.

Keywords: graphene, Dirac electrons, quantum dots, quasi-bound states

PACS: 73.63.Kv, 73.43.Cd, 81.05.Uw, 03.65.-w, 73.21.La

1. Introduction

During the last seven years, graphene (a single layer of carbon atoms) has become a very active field of research in nanophysics [1, 2] (see also [3] and references therein). This new ideal 2D (two-dimensional) system exhibits special excitations (electrons and holes) that are very similar to the relativistic particles described by the Dirac equation. Due to the so-called Klein effect [4] the control of their behaviour by means of electromagnetic fields is one of the most challenging tasks.

One of the most successful nanostructures for controlling electron and hole behaviour are the quantum dots (QDs) [5] that are confined quantum mechanical systems with a discrete energy spectrum, or the so-called "artificial atoms". Nonrelativistic electrons, the properties of which are described by the Schrödinger equation, can be easily confined by electrostatic confinement potentials. It is impossible to confine electrons in graphene into an electric QD due to the above-mentioned Klein effect. In this case we need to consider not the QD that localises an electron, i. e. in which the electron stays for an infinitely long time, but a QD that can trap the electron for a long enough time. From the experimental point of view such quasi-bound state is actually equivalent to the bound state in the QD.

The theory of a quasi-bound state has a long history. The first theory was developed by Gamow [6], and then improved by Gurney and Condon [7]. The most comprehensive explanation of its various properties was achieved via solution of simple models [8].

The quasi-bound states of QDs in graphene were described by means of a quasi-classical approach [9], which was successful in the case of QDs with a smooth confinement potential, and it was shown that electron trapping occurs in the case of a large angular momentum of the electron. The case with sharp QD borders was considered in Refs. [10] and [11].

The main task of this paper is to present the local density of states technique as a means for defining the quasi-bound state and to describe the way of its calculation by comparing the electric and magnetic circular dots with sharp borders for Schrödinger and Dirac electrons. Casually, we pursue two other pedagogic purposes. First, we draw attention to the analogy between 2D graphene and 1D chain models of polymers, which enables to explain the properties of graphene in the most simple way. Next, we consider a simple 1D model of a decaying state [8] for introducing the local density of states and showing the way of its calculation.

The layout of the paper is as follows: in Section 2 we explain the main features of graphene by means of its analogy to 1D chain models, in Section 3 the local density of states is introduced and the way of its calculation is discussed making use of a 1D model of a

decaying state. The Section 4 is devoted to the description of the electric QD, in Section 5 the magnetic QD for Schrödinger end Dirac electrons is discussed, and in the last Section 6 our conclusions are given.

2. 1D chain model

It is known that electrons and holes in graphene behave like relativistic particles and can be described by the Dirac equation. These features are mainly caused by a specific honeycomb graphene lattice, namely, two carbon atoms in a primitive cell and a half-filled conduction band. The most simple way to understand this behaviour is to exploit the analogy of graphene and a 1D chain model of polymer. So, following [12] we assume that there is a corrugated 1D lattice of carbon atoms shown in Fig. 1 like in a fixed molecule of trans-polyacetylene. It is characterised by the lattice constant

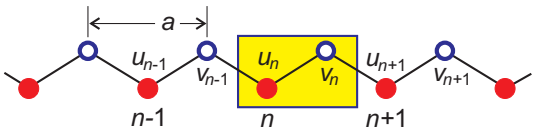

Fig. 1. (Colour online) Corrugated 1D lattice.

a and a primitive cell, shown by the shadowed rectanglein Fig. 1, containing two atoms. In the tight-binding approximation the motion of the electron in this lattice (the jumping between the neighbouring atoms) is described by the amplitudes u_n and v_n satisfying the following Schrödinger equation set:

$$i\frac{\partial}{\partial t}u_n = -i(v_{n-1} + v_n)\,, \tag{1a}$$

$$i\frac{\partial}{\partial t}v_n = i(u_n + u_{n+1})\,. \tag{1b}$$

Here and further we use the dimensionless units measuring all distances in lattice constants a, energy in units related to the tunneling amplitude W, and time in $\hbar/W$ units. It is convenient to present the above equations in a compact matrix form:

$$i\frac{\partial}{\partial t}\psi_n = H\psi_n\,, \quad \psi_n = \begin{pmatrix} u_n \\ v_n \end{pmatrix} \tag{2}$$

with Hamiltonian

$$H = i\begin{pmatrix} 0 & -1-T^{-1} \\ 1+T & 0 \end{pmatrix} \tag{3}$$

and the translation operator defined as

$$Tu_n = u_{n+1}, \quad Tv_n = v_{n+1}\,. \tag{4}$$

Choosing the amplitudes as

$$\begin{pmatrix} u_n(t) \\ v_n(t) \end{pmatrix} = \begin{pmatrix} u \\ v \end{pmatrix} e^{i(2kn-Et)} \tag{5}$$

that are in agreement with the lattice invariance in respect of time and coordinate translation and inserting them into Eqs. (1) we arrive at the following matrix equation:

$$E\begin{pmatrix} u \\ v \end{pmatrix} = i\begin{pmatrix} 0 & -1-e^{-2ik} \\ 1+e^{2ik} & 0 \end{pmatrix}\begin{pmatrix} u \\ v \end{pmatrix}. \tag{6}$$

At last, solving the above eigenvalue problem we obtain the electron spectrum

$$E_\pm = \pm\varepsilon(k) \equiv \mp 2\cos k\,. \tag{7}$$

It is shown in Fig. 2(a) by two crossing (red online) solid curves. These two spectrum branches are a con-

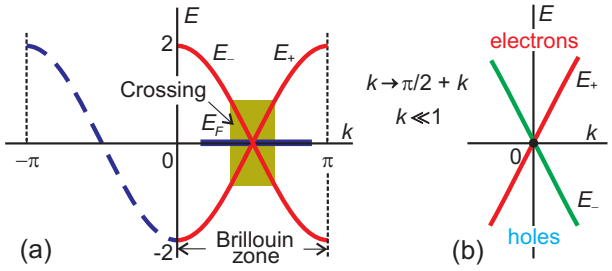

Fig. 2. (Colour online) (a) Electron spectrum for the corrugated 1D lattice. (b) Long wave approximation.

sequence of the chosen Brillouin zone ($0 < k < \pi$) related to the primitive cell with two atoms in it. If the lattice is not corrugated (like in polymer polyethylene) the primitive cell will be twice smaller (with just a single carbon atom in it), the Brillouin zone ($-\pi < k < \pi$) twice larger, and there will be just a single branch E_+ prolonged by the (blue online) dashed curve. In the corrugated lattice, this dashed piece of branch is just shifted to the right by π to the position of E_-. The crossing of spectrum branches, denoted by the shaded rectangle, is a consequence of a different symmetry of them. The reason is that the corrugated lattice has an additional symmetry: it can be translated by the distance $a/2$ with following inversion in the perpendicular direction (in crystallography such symmetry is known as a glide-reflection plane). That is why the spectrum branches can be distinguished by a certain additional quantum number $\kappa_\pm = \pm 1$ (the sign coincides with the energy sign in Eq. (7)) that is an analogue of chirality in a 2D graphene case.

There is one more important point that makes a 1D polyacetylene chain similar to a 2D graphene case.

This is band filling. The fact is that a carbon atom has four electrons in the outer shell, and only three of them participate in lattice formation. The last one goes into the calculated conduction band and half fills it. So, at zero temperature the Fermi energy E_F is exactly at the crossing point. In the case of low temperatures, only the states close to this crossing point are excited: the electrons above and the holes below it.

In graphene, the conduction band is about 20 eV wide. Thus room temperature, 300 K, is very low compared to this band width. For this reason, it is not necessary to take the entire energy band shown in Fig. 2(a) into account. Only a small shaded region shown separately in Fig. 2(b) (corresponding to the K points in graphene) is of importance. If for the sake of convenience we move the origin of the Brillouin zone to point $\pi/2$ (i. e. change $k \to k + \pi/2$), we have the spectrum consisting of two crossing linear branches with different chirality, as it is shown in Fig. 2(b). In this so-called long wave approximation ($k \ll 1$) the energy spectrum reads

$$E_{\pm}(k) = \mp 2\cos(\pi/2 + k) = \pm 2\sin k \approx \pm 2k\,, \quad (8)$$

and the matrix Hamiltonian (3) can be rewritten as

$$H = i\begin{pmatrix} 0 & -1-e^{-2i(k+\pi/2)} \\ 1+e^{2i(k+\pi/2)} & 0 \end{pmatrix} \approx 2\begin{pmatrix} 0 & k \\ k & 0 \end{pmatrix}. \quad (9)$$

This Hamiltonian acts on a (5) type wave function. To generalise it for any slowly varying wave function, we have to replace n by x, and the momentum $2k$ by its differential analogue $-i\partial k/\partial x$, what converts the above Hamiltonian into

$$H = \begin{pmatrix} 0 & -i\partial/\partial x \\ -i\partial/\partial x & 0 \end{pmatrix} = p_x \begin{pmatrix} 0 & 1 \\ 1 & 0 \end{pmatrix} = \sigma_x p_x\,, \quad (10)$$

where σ_x is the Pauli matrix. Equations (8) and (10) can be easily generalized for the 2D graphene case. Thus, replacing $\sigma_x p_x$ by the scalar product of 2D vectors $\mathbf{p} = \{p_x, p_y\}$ and $\sigma = \{\sigma_x, \sigma_y\}$ and going back to initial dimensions we have

$$E(\mathbf{k}) = \pm\hbar v_F|\mathbf{k}|, \quad H = v_F\sigma\cdot\mathbf{p}\,, \quad (11)$$

where v_F is the Fermi velocity that in the case of graphene is 10^6 m s^{-1}.

Using this analogy, the Klein effect becomes evident. Let us consider the penetration of a 1D electron into the electric barrier shown in Fig. 3 by the step-like (blue online) solid curve. The spectrum is shown schematically as well. We assume that the electron is

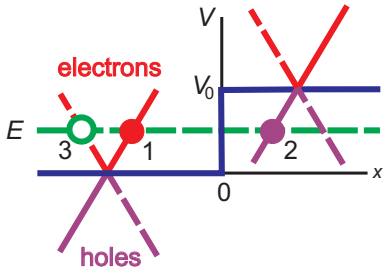

Fig. 3. (Colour online) 1D Dirac electron penetration into the electrical barrier.

coming from the left side of the barrier (its momentum is indicated by the (red online) solid circle 1) with energy E that is smaller than the barrier height V_0. In the standard Schrödinger case, the electron interacting with the barrier changes its momentum into that shown by the (green online) open circle *3*. In the above-considered Dirac electron case, however, this momentum change is forbidden due to the different chirality of both spectrum branches shown by solid and dashed curves. That is why there is just one way for the electron, namely, it can penetrate the barrier with the probability equal to unity, converting itself into a hole with the momentum indicated by the (violet online) solid circle *2*.

In the case of 2D graphene the transmission (or reflection) through the barrier is more complicated due to a more sophisticated chirality. The probability for the electron to pass the electric barrier has been studied in [4]. The result is shown in Fig. 4 in the directive pattern form. We see the incident angle dependence

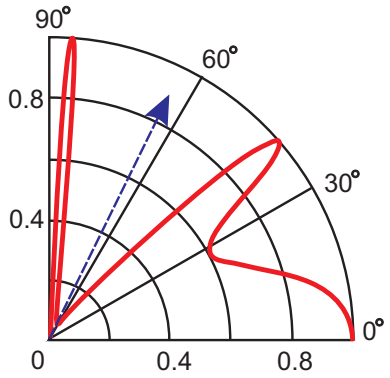

Fig. 4. (Colour online) 2D transmission through the electrical barrier, according to the results presented in [4].

of the probability for the electron to transmit the barrier of 100 nm width. The barrier height is 200 meV, and the energy of incoming electron is 80 meV. Due to the finite barrier width there are some angles at which the probability for the electron to transmit the barrier

is equal to unity. But for us the most important thing is that there are some angles (one of them indicated by the dashed (blue online) arrow) where this probability is rather small. Because of these angles with a small penetration probability there is a hope to trap the electron into the round electric dot if its angular momentum corresponds to these peculiar angles, and consequently, some quasi-bound states have to appear.

3. Local density of states

Before considering electron behaviour in a QD we have to decide what to calculate. Considering the finite systems such as quantum dots (QDs), or "hand made atoms", the main attention is paid to the electron spectrum, namely, the energy and eigenfunctions of the bound states. There are no bound states in a QD in graphene due to the above-mentioned Klein effect, and therefore it is necessary to deal with the quasi-bound states if there are ones. There is a hope that in this case the role of spectrum can be played by the local density of states. Indeed, when performing measurements we have to perturb the system by some external force. The main mathematical means to characterise the influence of this force is the golden Fermi rule defining the probability of some quantum transition of the electron system:

$$W = \frac{2\pi}{\hbar}|V|^2\rho(\varepsilon)\,. \tag{12}$$

Here V is the matrix element of the potential characterising the interaction of the system with the external force, and $\rho(\varepsilon)$ is the system density of states that describes its possibility to react to the above force. Formally, in the case of a finite system with the discrete energy spectrum, the above quantity is defined by means of the following sum of Dirac functions:

$$\rho(\varepsilon) = \sum_n \delta(\varepsilon - \varepsilon_n) \tag{13}$$

over all unperturbed system states. When apart from the spectrum the electron distribution is of interest, a more convenient quantity is the local density of states that is defined as the above sum weighted by the corresponding wave function squared

$$\rho(\varepsilon, \mathbf{r}) = \sum_n \delta(\varepsilon - \varepsilon_n)|\psi_n(\mathbf{r})|^2\,. \tag{14}$$

Generalising these both expressions we introduce the density of the states in the quantum dot

$$\rho_{\rm dot}(\varepsilon) = \sum_n \delta(\varepsilon - \varepsilon_n) \int {\rm d}^2 r\, f(\mathbf{r})\, |\psi_n(\mathbf{r})|^2\ , \tag{15}$$

where $f(\mathbf{r})$ is some aperture function characterising the interaction of electrons with the measuring probe. For instance, such quantity appears in the description of the tunneling current directed perpendicularly to the dot, or in the near-field infrared absorption by the QD.

In order to construct a calculation scheme for the above-introduced local density of states in a QD, it is worth to consider the most simple analytically solvable model of the decaying state [8] (see also [13] where various approximate methods are analysed). In this model the standard Schrödinger electron moves in the potential shown by the (blue online) solid curve in Fig. 5.

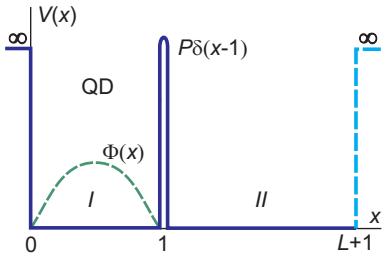

Fig. 5. (Colour online) Potential of the model 1D system.

This potential divides the positive x-half-axis (the region of 1D electron motion) into two parts. Part I ($0 < x < 1$) is actually the QD with the hard wall on its left side and separated by the Dirac function (weakly penetrable wall) from the infinite part II ($1 < x < \infty$). Due to this contact with part II, the QD is not stationary, and the electron inserted into it (say, by means of the initial condition $\Psi(x, 0) = \Phi(x)$) escapes to infinity sooner or later.

In order to apply the density of states definition (15) we include the additional hard wall at the point $x = L + 1$ (shown by the (light blue online) dashed curve) converting the system into the finite one. At the end of the calculation we shall take the limit $L \to \infty$ moving this additional wall to infinity and turning back to the initial infinite system with the continuous spectrum. Now we can apply the methods of spectrum analysis and solve the standard eigenvalue problem

$$(H - \varepsilon_n)\,\psi_n(x) = 0 \tag{16}$$

with the Hamiltonian

$$H = -\frac{1}{2}\frac{\partial^2}{\partial x^2} + V(x)\,. \tag{17}$$

The solution of the above equation in both parts (I and II) obeying the hard wall boundary conditions reads

$$\psi_n(x) = \begin{cases} A\sin(k_n x), & 0 < x < 1 \\ B\sin[k_n(x-L-1)], & 1 < x < L+1 \end{cases}, \tag{18}$$

corresponding to the eigenvalue $\varepsilon_n = k_n^2/2$. Assuming the wave function continuity at the QD border ($x = 1$) and replacing the Dirac function included into the potential by the corresponding boundary condition for the wave function derivative discontinuity, we obtain the following equation set of algebraic equations:

$$A\sin k_n = -B\sin(k_n L)\,, \tag{19a}$$

$$AD_n = B\cos(k_n L)\,, \tag{19b}$$

where

$$D_n = D(k_n), \quad D(k) = \cos k + \frac{2P}{k}\sin k\,. \tag{20}$$

Zeroing its determinant, we arrive at the equation

$$\tan(kL) = -\frac{1}{D(k)}\sin k \tag{21}$$

for the definition of eigenvalues k_n and energies ε_n.

Having in mind the normalisation of eigenfunction and the limit $L \to \infty$, we obtain the coefficient $B = \sqrt{2/L}$. Then the coefficient A follows from Eq. (19a):

$$A = -B\frac{\sin(k_n L)}{\sin k_n} = \frac{\sqrt{2/L}\,\tan(k_n L)}{\sin k_n\sqrt{1+\tan^2(k_n L)}}\,. \tag{22}$$

Assuming that the aperture function $f(x)$ is concentrated in the QD and inserting the eigenfunction (18) with the factor (22) into Eq. (15), we obtain the following definition of the local density of states in the QD:

$$\rho_{\rm dot}(\varepsilon) = \frac{2}{L}\sum_n \frac{\delta(\varepsilon-\varepsilon_n)\tan^2(k_n L)}{\sin^2 k_n\,[1+\tan^2(k_n L)]}C(k_n)\,, \tag{23}$$

where

$$C(k) = \int_0^1 {\rm d}x\, f(x)\sin^2(kx)\,. \tag{24}$$

The next step is to calculate the limit $L \to \infty$. It is necessary to pay attention to two points. First, according to Eq. (21) the eigenvalues k_n can be found as an intersection of rapidly oscillating tangent curves with a rather smooth curve in the right-hand side of that equation. Consequently, in the limit case the distance between the neighbouring eigenvalues can be estimated as $\Delta k_n = \pi/L$, and sum in Eq. (23) can be replaced by the integral as follows:

$$\sum_n \cdots = \frac{L}{\pi}\int {\rm d}k \cdots\,. \tag{25}$$

Next, this replacement can be performed only in the case if there are no rapidly oscillating terms. This is not the case, because there is a function $\tan(k_n L)$ in the right-hand side of Eq. (23). Fortunately, it can be eliminated due to dispersion relation (21). Performing this replacement we get

$$\rho_{\rm dot}(\varepsilon) = \frac{2}{L}\sum_n \frac{\delta(\varepsilon-\varepsilon_n)C(k_n)}{[D^2(k_n)+\sin^2 k_n]}$$

$$= \frac{2}{\pi}\int {\rm d}k \frac{\delta(\varepsilon-k^2/2)C(k)}{Q(k)} = \frac{2C(k)}{\pi k Q(k)}\bigg|_{k=\sqrt{2\varepsilon}}\,, \tag{26}$$

where

$$Q(k) = D^2(k) + \sin^2 k\,. \tag{27}$$

Due to a weak k-dependence of the coefficient $C(k)$, the function $Q^{-1}(k)$ determines the behaviour of the local density of states. In the case of $f(x) = 1$, it is shown in Fig. 6 for various P values. We see that

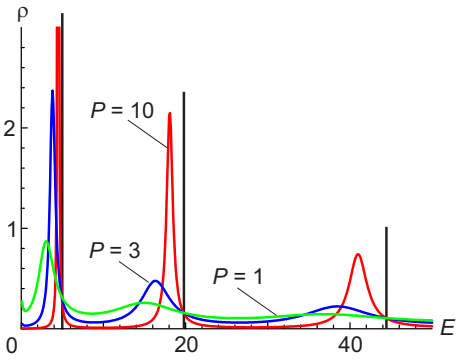

Fig. 6. (Colour online) Local density of the states in the QD.

when the value of P increases (when the right QD edge becomes less penetrable) the resonant curves become narrower approaching the energies of eigenstates of the isolated QD that are indicated by the solid (black online) vertical lines. In the $P \gg 1$ case, the curves become of Lorentzian type and their broadening (reciprocal lifetime) coincides with that obtained by a complex energy method or extracted from the exact solution (see, for instance, Ref. [13]).

Our main task is the calculation of the local density of states of electric and magnetic QDs in graphene by means of the above-presented method.

4. Electric quantum dot

We consider the QD in graphene following paper [14], i. e. solve the eigenvalue problem

$$\{H - E\}\Psi(\mathbf{r}) = 0 \tag{28}$$

with Hamiltonian (11) and the diagonal cylindrically symmetric electric potential

$$V(\mathbf{r}) = V\Theta(r - r_0) = \begin{cases} 0,\, 0 \leqslant r < r_0 \\ V, r_0 \leqslant r < \infty \end{cases} \tag{29}$$

added.

For the sake of convenience, we introduce dimensionless variables and measure the distances in the units of dot radius r_0 and energies in $\hbar v_F/r_0$ units. For instance, for a dot with radius $r_0 = 0.1\,\mu$m, the above energy unit is 6 meV.

Inserting a two-component wave function

$$\Psi(\mathbf{r}) = \begin{pmatrix} A(\mathbf{r}) \\ B(\mathbf{r}) \end{pmatrix} \tag{30}$$

into Eq. (28) we arrive at the following set of two equations:

$$\left(i\frac{\partial}{\partial x} + \frac{\partial}{\partial y}\right) B = -[E - V\Theta(r-1)]A\,, \tag{31a}$$

$$\left(-i\frac{\partial}{\partial x} + \frac{\partial}{\partial y}\right) A = [E - V\Theta(r-1)]B \tag{31b}$$

for the wave function components. Changing the variables $\{x, y\} \to \{r, \varphi\}$ and operators

$$\frac{\partial}{\partial x} - i\frac{\partial}{\partial y} = e^{-i\varphi}\left(\frac{\partial}{\partial r} - \frac{i}{r}\frac{\partial}{\partial \varphi}\right), \tag{32}$$

we rewrite Eqs. (31) as

$$[V\Theta(r-1) - E]A = ie^{-i\varphi}\left(\frac{\partial}{\partial r} - \frac{i}{r}\frac{\partial}{\partial \varphi}\right)B, \tag{33a}$$

$$[V\Theta(r-1) - E]\,B = ie^{i\varphi}\left(\frac{\partial}{\partial r} + \frac{i}{r}\frac{\partial}{\partial \varphi}\right)A\,. \tag{33b}$$

These equations can be further simplified by using the circle symmetry of our problem what enables to express the angular dependence of the wave function components explicitly:

$$\begin{pmatrix} A(\mathbf{r}) \\ B(\mathbf{r}) \end{pmatrix} = \begin{pmatrix} A(r,\varphi) \\ B(r,\varphi) \end{pmatrix} = e^{im\varphi}\begin{pmatrix} a(r) \\ ie^{i\varphi}b(r) \end{pmatrix}, \tag{34}$$

where the integer m stands for the eigenstate angular momentum. This assumption converts Eqs. (33) into the following set of coupled ordinary radial differential equations:

$$[V\Theta(r) - E)]\,a = -\left(\frac{\mathrm{d}}{\mathrm{d}r} + \frac{m+1}{r}\right)b\,, \tag{35a}$$

$$[V\Theta(r) - E)]\,b = \left(\frac{\mathrm{d}}{\mathrm{d}r} - \frac{m}{r}\right)a\,. \tag{35b}$$

These two equations have to be solved in the inner ($r < 1$) and outer ($1 < r$) region of the dot ensuring the continuity of both wave function components (a and b) at the quantum dot edge $r = 1$.

Inserting b from Eq. (35b) into Eq. (35a) we arrive at the second-order ordinary differential equation

$$\left(\frac{\mathrm{d}^2}{\mathrm{d}r^2} + \frac{1}{r}\frac{\mathrm{d}}{\mathrm{d}r} - \frac{m^2}{r^2}\right)a = -\left[V\Theta(r-1) - E\right]^2 a\,, \tag{36}$$

which actually coincides with the Bessel function equation. The other wave function component can be easily obtained from Eq. (35b). Thus, the solution inside the dot (where $V(r) = 0$) in the case of positive energy $E > 0$ reads

$$a = FJ_m(Er)\,, \tag{37a}$$

$$b = FJ_{m+1}(Er)\,. \tag{37b}$$

Note that we did not include the Bessel function of the second order $Y_m(Er)$ into our solution, as it is singular at the origin $r = 0$. Outside the dot ($1 < r$) the solution is

$$a = PJ_m(\kappa r) + QY_m(\kappa r)\,, \tag{38a}$$

$$b = \mp[PJ_{m+1}(\kappa r) + QY_{m+1}(\kappa r)]\,, \tag{38b}$$

where

$$\kappa = |E - V|\,, \tag{39}$$

and the sign in the right-hand side of the b expression coincides with the sign of $(E - V)$. Satisfying the boundary conditions at $r = 1$ we obtain two equations for the definition of three coefficients: F, P, and Q. Drawing attention to the linearity of these equations we see that they can be satisfied for any value of energy E. This fact means that the energy spectrum is continuous, and consequently, there are no bound states.

In order to find the possible quasi-bound states we shall follow the procedure presented in Section 3 and solve the eigenvalue problem in the finite circle with the radius R ($r < R$). At the end of our consideration we shall calculate the limit $R \to \infty$. The wave function components a and b are related to two carbon atoms in

the primitive cell of 2D graphene as it was in the 1D chain model discussed in Section 2. At the point $r = R$ there is either type a or b atom, and the single exact boundary condition depends on the actual configuration of atoms at the QD edge. We restrict our consideration, however, to the simple equation

$$a(R) = 0\,, \tag{40}$$

as the local density of states in the QD that we are looking for is not sensitive to the microscopic details of the auxiliary sample edge in the limit $R \to \infty$.

So, satisfying boundary conditions for a and b components at $r = 1$ and Eq. (40) we obtain the following set of algebraic equations for the coefficients:

$$FJ_m(E) = PJ_m(\kappa) + QY_m(\kappa)\,, \tag{41a}$$

$$FJ_{m+1}(E) = \mp[PJ_{m+1}(\kappa) + QY_{m+1}(\kappa)]\,, \tag{41b}$$

$$PJ_m(\kappa R) + QY_m(\kappa R) = 0\,. \tag{41c}$$

We see that there are fast and slow oscillating functions, as it was in the 1D case. As we are looking for the limit $R \to \infty$ the fast oscillating functions have to be eliminated. It is easy to do this by performing some steps similar to those we used in Section 3. We start with replacing the Bessel functions in Eq. (41c) by their asymptotic expressions, what results in

$$P\cos\left(\kappa R - \frac{\pi m}{2} - \frac{\pi}{4}\right) + Q\sin\left(\kappa R - \frac{\pi m}{2} - \frac{\pi}{4}\right) = 0\,. \tag{42}$$

It is evident that the solution of this equation can be chosen as

$$P = N\sin\left(\kappa R - \frac{\pi m}{2} - \frac{\pi}{4}\right)\,, \tag{43a}$$

$$Q = -N\cos\left(\kappa R - \frac{\pi m}{2} - \frac{\pi}{4}\right)\,. \tag{43b}$$

In the limiting case, $R \to \infty$, the normalisation factor N can be calculated just using the same asymptotic wave function expression, namely,

$$1 \approx 2\cdot 2\pi \int_0^R r\,\mathrm{d}r \left(\frac{2}{\pi\kappa r}\right)\left[P\cos\left(\kappa r - \frac{\pi m}{2} - \frac{\pi}{4}\right) + Q\sin\left(\kappa r - \frac{\pi m}{2} - \frac{\pi}{4}\right)\right]^2 = \frac{4N^2R}{\kappa}\,. \tag{44}$$

The additional factor 2 appears because both wave function components (a and b) have to be taken into account. Consequently, the normalisation factor reads

$$N = \sqrt{\frac{\kappa}{4R}}\,. \tag{45}$$

It follows from Eq. (43) that, first,

$$P^2 + Q^2 = \frac{\kappa}{4R}\,, \tag{46}$$

and next, the neighbouring eigenvalues are separated by

$$\Delta E = \Delta\kappa = \frac{\pi}{R}\,. \tag{47}$$

Now by analogy with Eq. (15) we define the local density of states in the round QD corresponding to the orbital momentum m as

$$\rho_{\mathrm{dot}}(E,m) = 2\pi\sum_n \delta(E - E_{m,n}) \int_0^1 r\,\mathrm{d}r\, f(r)\,[|a|^2 + |b|^2]\,. \tag{48}$$

Assuming that the aperture function $f(r)$ fits entirely in a dot, keeping in mind Eqs. (47) and (37), including normalisation N into the definition of all wave function coefficients, and calculating the limit $R \to \infty$ we rewrite the above equation as

$$\rho_{\mathrm{dot}}(E,m) = \frac{\kappa F^2}{2} \int_0^1 r\,\mathrm{d}r\, f(r)\,\left[J_m(Er)^2 + J_{m+1}(Er)^2\right]\,. \tag{49}$$

We see that within the accuracy of the experimental form-factor (the integral in the right-hand side of Eq. (49)) the quantity

$$\rho_{\mathrm{dot}}(E,m) = \frac{1}{2}|E - V|F^2 \tag{50}$$

acts as a local density of states in the quantum dot area. It is remarkable that the obtained local density of states consists of two factors. One of them, $|E - V|$, is just the density of states of a free 2D electron (or hole) in the barrier region, while the other one, F^2, is its modulation caused by the quantum dot itself.

We solved Eqs. (41a) and (41b) together with equation

$$P^2 + Q^2 = 1 \tag{51}$$

numerically from which we obtained the coefficient F and the local density of states in the QD (50). A typical

example for the two components of the wave function together with the confinement potential profile is shown in Fig. 7.

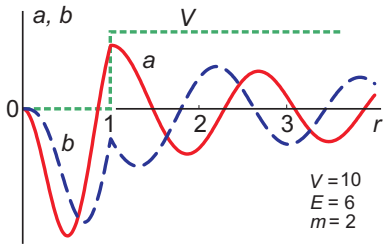

Fig. 7. (Colour online) Profile of the confinement potential ((green online) dotted curve), and the two wave function components: (red online) solid curve a, (blue online) dashed curve b. Barrier height $V = 10$, energy $E = 6$, and orbital momentum $m = 2$.

As the energy is lower than the potential height we see that two wave function components have a different phase indicating the electronic type character of the wave function inside the dot, and the hole type character outside it. The large value of the wave function components inside the dot shows that this eigenfunction corresponds to the quasi-bound state.

The typical local density of states is shown in Fig. 8. It exhibits peaks that can be associated with the quasi-

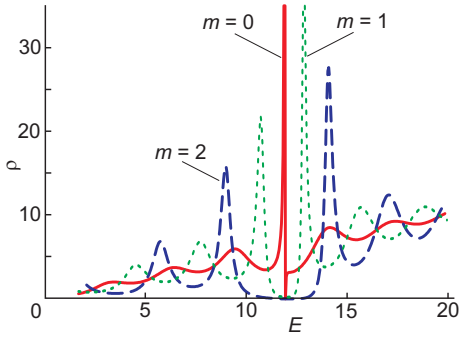

Fig. 8. (Colour online) Local density of states as a function of energy in case of barrier height $V = 12$ for the orbital momenta $m = 0$ ((red online) solid curve), $m = 1$ ((green online) dotted curve), and $m = 2$ ((blue online) dashed curve).

bound states of the dot. The increasing background can also be revealed, which is a consequence of the above-mentioned factor $|E - V|$ in Eq. (50) corresponding to the density of states of a free electron or hole in the barrier region. The three curves correspond to the orbital momenta of electron $m = 0, 1, 2$. We observe the general tendency that the larger the orbital momentum the narrower the peaks. A very narrow peak is observed when the energy is close to the barrier height (see the curve for $m = 0$). This tendency is even better seen in Figs. 9 and 10 where the positions and broadenings of the peaks are shown.

We fitted peaks in the density of states by Lorentzian functions $a_n\gamma_n/\{(E - E_n)^2 + \gamma_n^2\}$ defining three parameters for any of them: position E_n, its broadening γ_n, and amplitude a_n. Graphically, these parameters are shown in Figs. 9 and 10 for two orbital momentum m values as a function of the barrier height V.

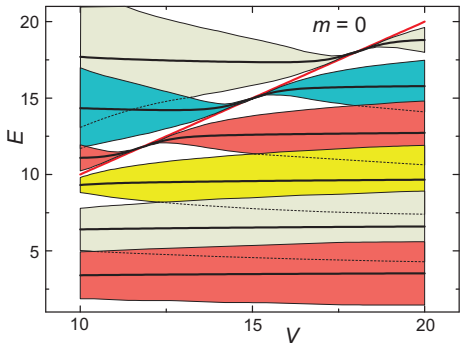

Fig. 9. (Colour online) Quasi-bound states with orbital momentum $m = 0$ for a quantum dot in graphene. The energy of these states is given by the solid curves, and their width (i. e. the inverse of the lifetime) by the shaded region. The straight (red online) slanted line corresponds to $E = V$.

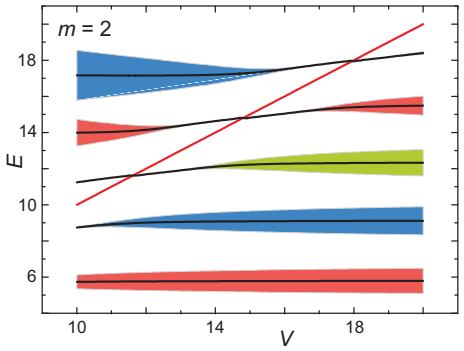

Fig. 10. (Colour online) Quasi-bound states with orbital momentum $m = 2$ for a quantum dot in graphene. The energy of these states is given by the solid curves, and their width (i. e. the inverse of the lifetime) by the shaded region. The straight (red online) slanted line corresponds to $E = V$.

The positions E_n of the quasi-bound levels are shown by the solid curves while the shaded areas between two $E_n \pm \gamma_n$ curves indicate the broadening of them. As expected, in the case $m = 0$ the levels are rather broad. Actually, they can hardly be identified as quasi-bound levels and rather correspond to weak oscillations in the local density of states of the continuous spectrum (see the solid curve in Fig. 8).

In the case of $m = 2$ we see (Fig. 10) a quite different picture. The levels are narrow and indicate the presence of long living quasi-bound states. It is interesting to see that the quasi-bound states are seen above as well as below the barrier, the latter is indicated by the slant solid line. Actually, this is the consequence of the equivalence of the Dirac electrons and holes in the barrier region.

As has already been mentioned, in Figs. 9 and 10 we see one more important peculiarity of the local density of states of a QD in graphene, i. e. extremely narrow states in the vicinity of the top of the barrier. This is not an accidental phenomenon, but the consequence of an important fact that it is rather difficult for Dirac electrons to penetrate the barrier when its energy is close to the barrier height. This property follows straightforwardly from the problem of electron penetration through the barrier solved in [4], although the authors paid no attention to this limit case. The fact is that the angle φ (with respect to the perpendicular to the barrier) of the incident electron and the angle ψ of the refracted electron have to satisfy the equation

$$E \sin\varphi = (V - E) \sin\psi \,, \tag{52}$$

which is the equivalent of Snell's law in optics [15]. In the case when electron energy is close to the barrier height,

$$|V - E| \ll V \tag{53}$$

the electron wave goes from the material with a large refraction index into the material with a small one. In this case the well-known phenomenon of total internal reflection takes place. It means that there is a critical incident angle

$$\varphi_0 = |V - E|/V \tag{54}$$

such that electrons with incident angles $|\varphi| > \varphi_0$ are totally reflected from the barrier. So, when electron energy is close to the barrier height there is only a very small region of incident angles at which the electron can penetrate the barrier, and this actually enhances electron confinement in the QD and makes its lifetime quite long even for the zero orbital momentum.

5. Magnetic quantum dot

In this Section we consider a possibility to localise electrons by an inhomogeneous magnetic structure, namely, in a magnetic QD, or in a certain region with the magnetic field when there is no field around it. It is known that the inhomogeneity of the magnetic field binds electrons, forming the so-called skipping orbits (see for instance [16]). The edge states are a quantum mechanical analogue of them. The simplest example of these edge states appears close to the magnetic step discussed in [17]. It is not difficult to imagine that a magnetic field created in a certain finite region of the plane forces electrons to move along the edge of this region and localises them in such way. The task of this Section is to check this possibility. Following the paper [18] we considered a model homogeneous magnetic field that is non-zero in a circle ,

$$\mathbf{B}(\mathbf{r}) = \{0, 0, B_0\}\Theta(r_0 - r) \,, \tag{55}$$

that we call the magnetic quantum dot. Because of the cylindric symmetry of the problem we choose the symmetric gauge for the vector potential defining its single azimuthal component as

$$A_\varphi(r) = \frac{1}{2}\begin{cases} r, & r < r_0 \\ r_0^2/r, & r_0 < r \end{cases} \,. \tag{56}$$

This azimuthal component is shown in Fig. 11 together with the magnetic field profile. In this Section we use

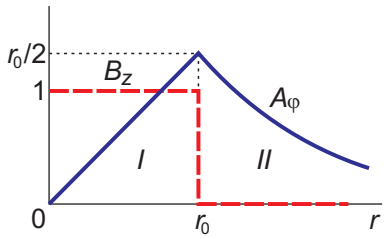

Fig. 11. (Colour online) Azimuthal vector potential component A_φ ((blue online) solid curve) and perpendicular magnetic field B_z ((red online) dashed curve) as functions of the radial coordinate.

the dimensionless variables based on the magnetic field strength value B_0. Thus, the magnetic field $B(\mathbf{r})$ is measured in B_0 units; all distances are measured in the unit of magnetic length $l_B = \sqrt{c\hbar/eB_0}$, and the vector potential in $B_0 l_B$ units.

5.1. Electron with parabolic energy dispersion

We start our consideration of the magnetic QD with the standard 2D electron (say, the electron moving at a GaAs/AlGaAs interface) with parabolic energy dispersion. In this case we add to the above-mentioned units the energy unit $\hbar\omega_c$ ($\omega_c = eB_0/mc$). Thus, when the magnetic field is of 1 T and effective mass is $m^* = 0.067$, the unit of length is $l_B = 250$ nm, and the energy unit is 20 meV.

So, we solve the stationary Schrödinger equation (28) with the following dimensionless Hamiltonian

$$H = -\frac{1}{2}\left(\nabla + i\mathbf{A}\right)^2 . \tag{57}$$

The stationary Schrödinger equation in cylindric coordinates reads

$$\left[\frac{1}{r}\frac{\partial}{\partial r}r\frac{\partial}{\partial r} + \frac{1}{r^2}\frac{\partial^2}{\partial\varphi^2} + \frac{iA_\varphi}{r}\frac{\partial}{\partial\varphi} - A_\varphi^2 + 2E\right]\Psi = 0 . \tag{58}$$

Substituting the wave function

$$\Psi \equiv \Psi(r,\varphi) = e^{im\varphi}\psi(r) \tag{59}$$

we arrive at the radial equations

$$\left[\frac{1}{r}\frac{\mathrm{d}}{\mathrm{d}r}r\frac{\mathrm{d}}{\mathrm{d}r} - \left(\frac{m}{r}+\frac{r}{2}\right)^2 + 2E\right]\psi_I(r) = 0 , \tag{60a}$$

$$\left[\frac{1}{r}\frac{\mathrm{d}}{\mathrm{d}r}r\frac{\mathrm{d}}{\mathrm{d}r} - \frac{(m+r_0^2/2)^2}{r^2} + 2E\right]\psi_{II}(r) = 0 , \tag{60b}$$

that have to be solved inside the dot (region I) and outside it (region II). The boundary conditions (continuity of the wave function and its radial derivative) have to be satisfied at the dot border ($r = r_0$).

The regular solution inside the dot can be expressed via the confluent hypergeometric function (Kummer function $M(a|c|z)$):

$$\psi_I(r) = Ag(r) = Ar^{|m|}e^{-r^2/4} \times M\left(\frac{|m|+m+1}{2} - E \,\middle|\, |m|+1 \,\middle|\, \frac{r^2}{2}\right), \tag{61}$$

while the solution outside it is composed of two Bessel functions,

$$\psi_{II}(r) = BJ_\nu(kr) + CY_\nu(kr) , \tag{62}$$

where $k = \sqrt{2E}$ is the momentum of the free electron (measured in l_B^{-1} units), and $\nu = m + r_0^2/2$. Note that both functions (J_ν and Y_ν) suit us, as they vanish in the limit $r \to \infty$.

So, we have the same problem as in the case of the electric QD (see the comment below Eq. (39)). We have three coefficients A, B, and C. They can be defined for any energy value. That is why we have to conclude that there are no bound states, and consequently, a magnetic field in a finite region of the 2D plane cannot confine the electron. However, quasi-bound states can be expected when electron energy in the dot is close to the Landau levels with energy

$$E_{n,m} = n + \frac{|m|+m+1}{2} \tag{63}$$

(here $n = 0, 1, \cdots$ and $m = 0, \pm1, \cdots$) defined in the case of a homogeneous magnetic field. The confirmation of this statement follows from Fig. 12, where the electron wave functions for two different energies are shown. We see that in the case of $E = 2.5$ (solid

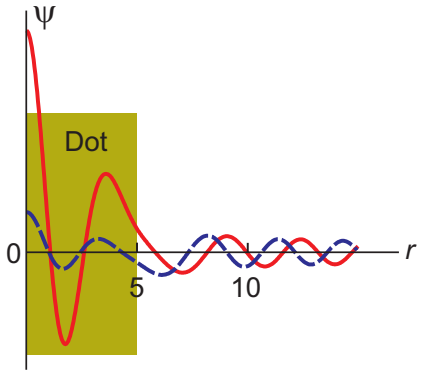

Fig. 12. (Colour online) The wave functions for $m = 0$, $r_0 = 5$: $E = 2.5$ ((red online) solid curve) and $E = 2.8$ ((blue online) dashed curve). The magnetic dot region is indicated by shaded rectangle.

curve), which corresponds to the Landau level with $n = 2$ and $m = 0$, the wave function is large in the dot region (shaded rectangle), while in the case of energy $E = 2.8$ (dashed curve), which does not coincide with any Landau level energy, it does not have any appreciable large value inside the dot and actually does not differ much from the wave function for a free electron calculated in cylindric coordinates.

Applying the technique described in the previous Section we calculated the local density of states. As in the case of the electric dot we confined the electron in a large region of the finite radius R, where its wave function obeyed the zero boundary condition at the border ($r = R$). Consequently, we had to solve the following set of equations that are similar to Eq. (41):

$$Ag(r_0) = BJ_\nu(kr_0) + CY_\nu(kr_0) , \tag{64a}$$

$$Ag_r(r_0) = BJ_{\nu,r}(kr_0) + CY_{\nu,r}(kr_0) , \tag{64b}$$

$$BJ_\nu(kR) + CY_\nu(kR) = 0 , \tag{64c}$$

where subindex r stands for the function radial derivative.

When solving Eq. (64c) in the asymptotic region ($R \to \infty$), calculating the normalisation constant

$$N = \sqrt{\frac{k}{2R}} , \tag{65}$$

assuming that the aperture function $f(r)$ fits entirely in a dot, and including the above norm into the definition of the local density of states, we present it in the form analogous to Eq. (48):

$$\rho_{\rm dot}(E,m) = \frac{\pi k A^2}{R} \sum_n \delta(E-E_{m,n}) \int_0^1 r\,{\rm d}r\, f(r)\, g^2(r)\,, \qquad (66)$$

where the coefficient A has to be found solving Eqs. (64a) and (64b) together with equation

$$B^2 + C^2 = 1\,. \qquad (67)$$

The solution of this equation set actually reduces to the numerical evaluation of the Kummer and Bessel functions.

Having in mind the separation between the neighbouring state energies

$$\Delta E = k\Delta k = k\frac{\pi}{R}\,, \qquad (68)$$

we convert the summation into integration and write down the final expression for the local density of states that we are looking for:

$$\rho_{\rm dot}(E,m) = A^2 \int_0^1 r\,{\rm d}r\, f(r)\, g^2(r)\,. \qquad (69)$$

We see that the result is identical to the one obtained in the previous Section, namely, with the accuracy of the form-factor that characterises the interaction of the QD with the measuring probe, the local density of states is given by the coefficient A squared (the averaged value of the proper normalised wave function squared in the QD). The quantity A^2 is sensitive to the probability to find the electron in the dot, and in the case of a quasi-bound state it will exhibit a peak corresponding to the approximate energy of this state, as it is shown in Fig. 13 where a typical result for the local density of states as a function of electron energy is given by the solid curve. The form-factor was evaluated using the Gaussian aperture function

$$f(r) = b\, r_0^2\, e^{-br^2}, \quad b = r_0^{-2}\,\ln 10\,, \qquad (70)$$

which corresponds to the averaged probability to find the electron in the dot area πr_0^2.

We clearly see peaks close to the energies of the Landau levels (63) calculated for the case of a homogeneous magnetic field. These peaks are broadened indicating that they are not really bound states in the magnetic dot. The broadening is larger for higher energy peaks.

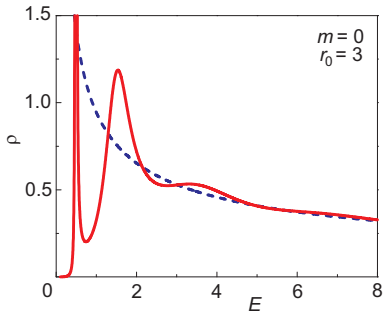

Fig. 13. (Colour online) The local density of states for $m = 0$ and $r_0 = 3$ shown by the solid curve. The same density calculated for a free electron according to Eq. (72) is shown by the dashed curve.

The next thing that is also seen in Fig. 13 is the background decreasing with energy. This background is due to the states of the free electron in the absence of the magnetic dot. To justify this statement we made the same calculation by replacing the radial parts of the wave function given by Eqs. (61) and (62) by the radial component of the free electron wave function (when there is no magnetic dot) that reads

$$\psi_{\rm free}(r) = J_m(kr) \qquad (71)$$

and is valid in the whole 2D plane. Averaging it with the same aperture function (70) we obtained the local density of states for a free electron

$$\rho_{\rm free}(E) = \frac{r_0^2}{2}\, e^{-E/b}\, I_m(E/b)\,, \qquad (72)$$

where $I_m(x)$ stands for the modified Bessel function of the first kind. This local density of a free electron in the case of $m = 0$ is shown in the same Fig. 13 by the dashed curve. Comparing these two curves, we clearly see how by increasing the electron energy we reduce the influence of the magnetic dot on the electron behaviour and the local density of states converts itself gradually into the free electron one.

Following the ideas of Section 4 we fitted the peaks in the density of states by Lorentzian functions and present the obtained parameters for $m = 0$ in Fig. 14 as functions of the radius of the dot r_0 like it was shown in Fig. 9 for the case of the electric QD. Actually, it gives the dependence of peak parameters on the strength of the magnetic field B because in the used dimensionless notations the distances are measured in the units of magnetic length. Going back to original notations we have to replace r_0 by $r_0/l_B \sim r_0\sqrt{B}$.

Note that the levels to the right of the dotted curve are extremely narrow and their position coincides with

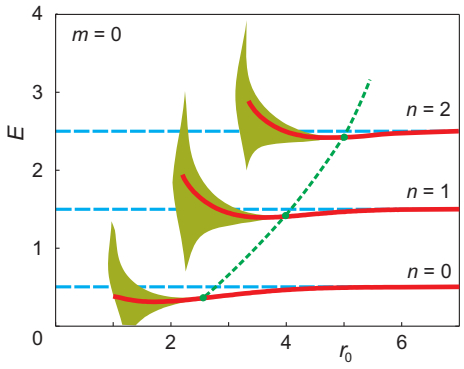

Fig. 14. (Colour online) Quasi-bound states with the orbital momentum $m = 0$. The energies of these states are given by solid curves and the widths (i. e. the inverse of the lifetime) by shadowed regions. The Landau levels are indicated by horizontal dashed lines.

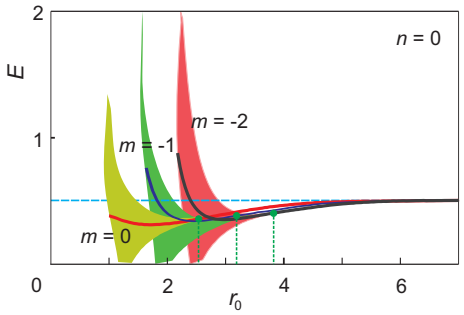

Fig. 15. (Colour online) The lowest quasi-bound state with $n = 0$ and different negative m values. The vertical (green online) dotted lines are the analogue of the dotted curve in Fig. 14, separating the weakly broadened states from those with a small lifetime.

the Landau levels (63) shown by the dashed horizontal lines. In fact, this means that almost the whole electron wave function is located in the magnetic dot (using the classical description language we may say that the electron rotates along the Larmor circle inside the dot) and it does not touch the border of it. When the dot radius r_0 becomes smaller, the Larmor circle touches the dot border and the tunnelling of the electron outside the dot starts which broadens the level. The partial penetration of the wave function outside the dot leads to the lowering of the quasi-bound state energy as well. The raising of this energy for small r_0 values is caused by a large asymmetry of the peak where actually the approximate replacement of the peak by a Lorentzian type function is no longer valid. This picture is more or less the same for all positive m values. The only difference is that for larger m values the levels start at higher energies what is in agreement with the expression for Landau levels (63).

The picture for negative m values is different (see Fig. 15). All of them belong to the same Landau level energy which is an expression of the degeneracy of the Landau level. We see that with the radius of the dot r_0 decreasing the levels with different m disappear gradually: the ones with smaller absolute m values disappear later. This is in agreement with the fact that the larger the $|m|$ value the larger the radius of the electron trajectory and the closer the electron wave function to the dot edge.

The increase of the peak broadening at small r_0 values is so steep that it is worth to divide all the peaks into two classes as shown in the above figures by the (green online) dotted curves.The levels on the left side of these curves belong to essentially broadened quasi-bound states, while from the experimental point of view those on the right side can hardly be distinguished from the real bound states. One can rudely estimate the position of the boarder by comparing the approximate dimensions of the electron wave function calculated in the case of a homogeneous magnetic field (which actually coincides with the function (61) extended to the entire plane) with the magnetic dot radius r_0.

5.2. Dirac electron in graphene

In this Section we repeat the above calculation for the magnetic dot applying it to the case of a Dirac electron in graphene, where the low-energy quasi-particles (electrons and holes) are described by the following dimensionless Dirac-like Hamiltonian:

$$H = \sigma\left(-i\nabla + \mathbf{A}\right) , \tag{73}$$

which is made of Eq. (11) with the vector potential added. The units are based on the magnetic field strength B_0 and are the same as in the previous Section, except for the unit of energy that is $v_F\hbar/l_B$ with the Fermi velocity $v_F = 10^8$ cm s^{-1}. In the case of a 1 T magnetic field, this energy unit is 2.6 meV. The vector potential is given by Eq. (56) and shown in Fig. 11.

The approach is based on the same stationary Schrödinger equation (28) used in Section 4, but with the matrix Hamiltonian (73). Assuming the two-component wave function given by Eqs. (30) and (34) we arrive at the following set of radial equations:

$$\left[\frac{\mathrm{d}}{\mathrm{d}r} + A(r) + \frac{m+1}{r}\right] b = Ea\,, \tag{74a}$$

$$-\left[\frac{\mathrm{d}}{\mathrm{d}r} - A(r) - \frac{m}{r}\right] a = Eb\,, \tag{74b}$$

that has to be solved in two regions (in the dot region I, and outside it, in region II). We require the continuity of the obtained components at the dot border r_0:

$$a_I(r_0) = a_{II}(r_0), \quad b_I(r_0) = b_{II}(r_0)\,. \tag{75}$$

In a standard way we convert Eqs. (74) into second-order differential equations for a single component, say for component b,

$$\left\{\frac{1}{r}\frac{\mathrm{d}}{\mathrm{d}r}r\frac{\mathrm{d}}{\mathrm{d}r} - \frac{(m+1)^2}{r^2} - \frac{r^2}{4} + \left[E^2 - m\right]\right\} b_I = 0\,, \tag{76a}$$

$$\left\{\frac{1}{r}\frac{\mathrm{d}}{\mathrm{d}r}r\frac{\mathrm{d}}{\mathrm{d}r} + \left[E^2 - \frac{(m+1+r_0^2/2)^2}{r^2}\right]\right\} b_{II} = 0\,. \tag{76b}$$

In contrast to the case of the electric quantum dot which was considered in Section 4, the effective potential (namely, vector potential) in Eqs. (76) is a continuous function at the dot border. For this reason the boundary conditions (75) are equivalent to the continuity of the wave function component itself and its first radial derivative

$$b_I(r_0) = b_{II}(r_0), \quad b_{I,r}(r_0) = b_{II,r}(r_0)\,. \tag{77}$$

The equations (76) and boundary conditions are similar to those used for the description of the Schrödinger electron in Section 5.1. It enables us to use the full analogy with the previous case. Taking this analogy into account we have the following solution in both regions:

$$b_I(r) = Ag(r) = Ar^{|m+1|}e^{-r^2/4}M(a_0|c_0|r^2/2)\,, \tag{78a}$$

$$b_{II}(r) = BJ_\nu(kr) + CY_\nu(kr)\,, \tag{78b}$$

where $k = |E|$, $a_0 = (|m+1| + m + 1 - E^2)/2$, $\nu = m+1+r_0^2/2$, and $c_0 = |m+1|+1$. The expressions for the other wave function component $a(r)$ follow directly from Eq. (74a):

$$a_I(r) = Ah(r) = \frac{A}{E}r^{|m+1|}e^{-r^2/4}$$

$$\times\left[\frac{\mathrm{d}}{\mathrm{d}r} + \frac{|m+1|+m+1}{r}\right]M(a_0|c_0|r^2/2)\,, \tag{79a}$$

$$a_{II}(r) = BJ_{\nu-1}(kr) + CY_{\nu-1}(kr)\,. \tag{79b}$$

The wave function components obtained in the above way are illustrated in Fig. 16 for two different values of energy. We see the same tendency as in the case of the Schrödinger electron. When energy is close to the Landau level energy of the Dirac electron in a homogeneous magnetic field,

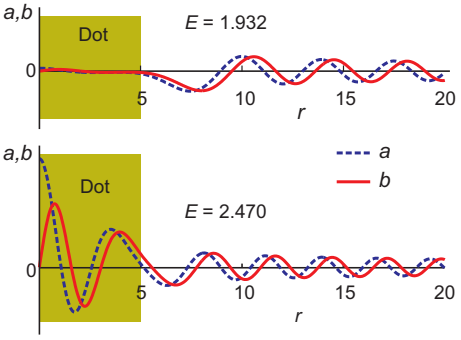

Fig. 16. (Colour online) The wave function components: a ((blue online) dashed) curve, and b ((red online) solid curve), for $m = 0$, dot radius $r_0 = 5$ and two energy values: $E = 1.932$ (upper plot), $E = 2.470$ (lower plot).

$$E_{n,m} = \pm\sqrt{2n + |m+1| + m + 1}\,, \tag{80}$$

(see the lower plot of Fig. 16 where energy is close to the Landau level with $m = 0$, $n = 2$) we see a clear accumulation of the wave function components in the dot, what indicates a quasi-bound state.

Using the analogy of Eq. (76) with the previously considered Eq. (36) in the case of the electric QD and paying attention that separation between the neighbouring state energies is $\Delta E = \Delta k = \pi/R$ (instead of Eq. (68)) we define the local density of states as

$$\rho_{\mathrm{dot}}(E,m) =$$

$$\frac{A^2|E|}{2}\int_0^1 r\,\mathrm{d}r\, f(r)\left[|a_I|^2(r) + |b_I|^2(r)\right]. \tag{81}$$

In order to define the coefficient A, one has to solve two equations following from boundary conditions (77) with Eq. (67) added.

In the case of free Dirac electrons (when there is no magnetic dot) the wave function components read

$$a_{\mathrm{free}} = J_m(kr), \quad b_{\mathrm{free}} = J_{m+1}(kr)\,, \tag{82}$$

what leads to the following expression of the local density of states for a free electron:

$$\rho_{\mathrm{free}}(E) =$$

$$\frac{|E|r_0^2}{4}e^{-E^2/2b}\left[I_m(E^2/2b) + I_{m+1}(E^2/2b)\right]. \tag{83}$$

The typical local density of states calculated for $m = 0$ and $r_0 = 3$ is shown in Fig. 17 for positive energies.

Two differences with respect to standard electrons can

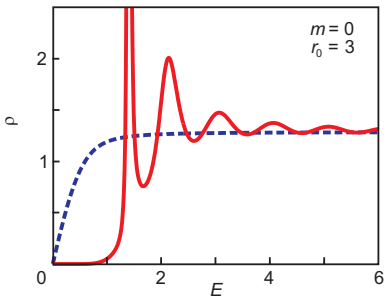

Fig. 17. (Colour online) The local density of states for a Dirac electron in the magnetic dot for $m = 0$ and $r_0 = 3$ shown by the (red online) solid curve. The (blue online) dashed curve is the free electron density of states (83).

clearly be noticed. First, in the case of the Dirac electron the spectrum is symmetric with respect to energy inversion ($E \to -E$) due to the equivalence of electrons and holes. Thus the plot in Fig. 17 has to be supplemented by the same curves for negative energies. Second, when comparing the density of states for the Dirac electron with the same curve for the Schrödinger one (see Fig. 13) we see that there are more peaks. This can be explained by a more dense Landau level spectrum in the case of Dirac electrons for the large quantum number values as compared with these in the previous case (compare Eqs. (80) and (63)).

As before, we fitted the peaks by Lorentz type curves what led to the broadened levels displayed in Figs. 18 and 19. The dotted curves divide the region of

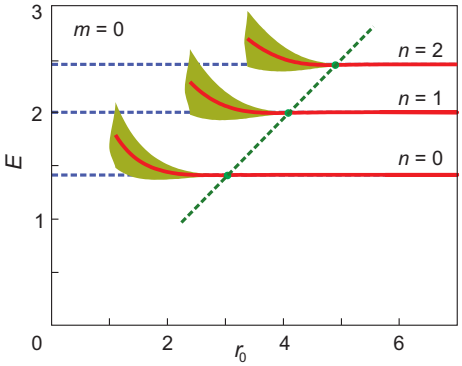

Fig. 18. (Colour online) Quasi-bound states with the orbital momentum $m = 0$ for the Dirac electron in the magnetic dot. The energy of these states is given by (red online) solid curves and their width (i. e. the inverse of the lifetime) by the shaded regions. The Landau levels are indicated by (blue online) dashed lines.

broadened quasi-bound states from the region where the states have a very small broadening.

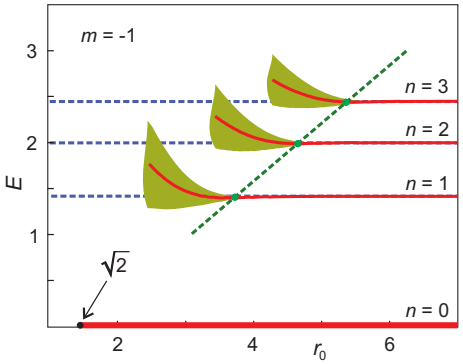

Fig. 19. (Colour online) Quasi-bound states with the orbital momentum $m = -1$ for the Dirac electron in the magnetic dot. The energy of these states is given by (red online) solid curves and their width (i. e. the inverse of the lifetime) by the shaded regions. The Landau levels are indicated by (blue online) dashed lines.

Note that in the case of $m = -1$ there is a zero energy state shown in Fig. 19 by the thick line along the r_0-axis. Its behaviour differs essentially from all other states. That is why it needs some special attention. In this case instead of Eqs. (74) we have to solve the following two equations for the radial components of the electron wave function:

$$\left[\frac{\mathrm{d}}{\mathrm{d}r} + A(r) + \frac{m+1}{r}\right] b = 0\,, \tag{84a}$$

$$\left[\frac{\mathrm{d}}{\mathrm{d}r} - A(r) - \frac{m}{r}\right] a = 0\,. \tag{84b}$$

These equations are uncoupled differential equations of the first order, and their solution can be found by a straightforward integration. The solution has the following asymptotic behaviour:

$$\ln a(r) = \int \mathrm{d}r \left[A(r) + \frac{m}{r}\right]$$

$$\sim \begin{cases} m \ln r + r^2/4\,, & r \to 0 \\ (m + r_0^2/2) \ln r\,, r \to \infty \end{cases} \tag{85}$$

and

$$\ln b(r) = -\int \mathrm{d}r \left[A(r) + \frac{m+1}{r}\right]$$

$$\sim \begin{cases} -(m+1) \ln r - r^2/4\,, r \to 0 \\ -(m + 1 + r_0^2/2) \ln r\,, r \to \infty \end{cases} \tag{86}$$

or

$$a(r) \sim \begin{cases} r^m \exp(r^2/4)\,, r \to 0 \\ r^{m+r_0^2/2}\,, \qquad r \to \infty \end{cases} \tag{87}$$

and

$$b(r) \sim \begin{cases} r^{-m-1} \exp(-r^2/4)\,, r \to 0 \\ r^{-(m+1+r_0^2/2)}\,, \qquad r \to \infty \end{cases} . \tag{88}$$

In order to have a wave function with the finite norm, two boundary conditions have to be satisfied. First, the function should behave like r^α ($\alpha \geqslant 0$) when $r \to 0$, and second, it should behave like $r^{-\beta}$ ($\beta \leqslant -1$) when $r \to \infty$.

For the a component the above conditions reduce to the requirements $m \geqslant 0$ and $m + r_0^2/2 \leqslant -1$, which cannot be satisfied simultaneously. Consequently, we have to assume that $a = 0$.

In the case of component b the conditions read

$$-r_0^2/2 \leqslant m \leqslant -1\,, \tag{89}$$

from which it follows that if $r_0^2/2 \geq 1$ there are always some negative m values for which the zero energy state exists. When the radius of the dot decreases this interval becomes smaller and the zero energy states vanish one by one. Finally, at $r_0 < \sqrt{2}$ all of them disappear.

Such essential difference between the bound zero energy level and all other quasi-bound levels is caused by the fact that the wave function of the state with zero energy is real. Consequently, the electron in this state has no velocity, and as a result there is no tunnelling of this electron outside the dot. Unfortunately, the absence of any non-zero electron velocity makes it impossible to reveal this state in transport measurements, but maybe it can reveal itself through the statistic properties of the magnetic dot.

6. Conclusions

The performed analysis of the behaviour of Schrödinger and Dirac electrons in electric and magnetic quantum dots enables us to make the following conclusions.

- The main features of the electron spectrum in graphene have analogy to those in 1D chains peculiar to polymers. These simple models can be useful for the understanding and interpretation of the sophisticated features of graphene.
- The quantum dots in graphene have no bound states. But there is a possibility for quasi-bound states to appear. The characteristics of a quasi-bound state, such as approximate energy or lifetime, can be found analysing the local density of states that is calculated by solving the eigenvalue problem for the finite system restricted at large distances.
- The quasi-bound states appear in an electric quantum dot in graphene in spite of the Klein effect. The lifetime of them is larger for the states with a larger orbital momentum. The states with the extremely long lifetime appear close to the top of the barrier what is the result of the total internal reflection, the analogue of the effect known in optics.
- Only a straight step of the magnetic field bounds electrons forming the edge states. They cannot be realised in the case of a bent step. As a consequence, the magnetic quantum dot has no bound states either for an ultra-relativistic Dirac electron in graphene or in the case of the Schrödinger electron with the parabolic energy dispersion law. However, the quasi-bound states could appear close to the Landau levels for the electron in the homogeneous magnetic field. The lifetime of them is quite long if the Larmor radius does not exceed the radius of the quantum dot.
- There are two differences between the states in the magnetic QD for Schrödinger and Dirac electrons. First, the spectrum of Schrödinger electrons is positive ($E > 0$), while in the case of Dirac electrons it is symmetric in respect of energy inversion ($E \to -E$). Besides, in the case of Dirac electrons there is a bound zero energy state the degeneracy of which goes down stepwise when the dot radius (or the strength of the magnetic field) decreases.

References

[1] K.S. Novoselov, A.K. Geim, S.V. Morozov, D. Jiang, M.I. Katsnelson, I.V. Grigorieva, S.V. Dubonos, and A.A. Firsov, Two-dimensional gas of massless Dirac fermions in graphene, Nature (London) **438**, 197 (2005), http://dx.doi.org/10.1038/nature04233

[2] Y. Zhang, Y.W. Tan, H.T. Stormer, and P. Kim, Experimental observation of the quantum Hall effect and Berry's phase in graphene, Nature (London) **438**, 201 (2005), http://dx.doi.org/10.1038/nature04235

[3] D.S.L. Abergel, V. Apalkov, J. Berashevich, K. Ziegler, and T. Chakraborty, Properties of graphene: a theoretical perspective, Adv. Phys. **59**, 261 (2010), http://dx.doi.org/10.1080/00018732.2010.487978

[4] M.I. Katsnelson, K.S. Novoselov, and A.K. Geim, Chiral tunnelling and the Klein paradox in graphene, Nat. Phys. **2**, 620–625 (2006), http://dx.doi.org/10.1038/nphys384

[5] T. Chakraborty, *Quantum Dots* (Elsevier, Amsterdam, 1999)

[6] G. Gamow, Zur Quantentheorie des Atomkernes, Z. Physik **51**, 204 (1928), http://dx.doi.org/10.1007/BF01343196

[7] R.W. Gurney and E.U. Condon, Quantum mechanics and radioactive disintegration, Phys. Rev. **33**, 127 (1929), http://dx.doi.org/10.1103/PhysRev.33.127

[8] R.G. Winter, Evolution of a quasi-stationary state, Phys. Rev. **123**, 1503 (1961), http://dx.doi.org/10.1103/PhysRev.123.1503

[9] P.G. Silvestrov and K.B. Efetov, Quantum dots in graphene, Phys. Rev. Lett. **98**, 016802 (2007), http://dx.doi.org/10.1103/PhysRevLett.98.016802

[10] P. Hewageegana and V. Apalkov, Electron localization in graphene quantum dots, Phys. Rev. B **77**, 245426 (2008), http://dx.doi.org/

[11] P. Hewageegana and V. Apalkov, Trapping of an electron in coupled quantum dots in graphene, Phys. Rev. B **79**, 115418 (2009), http://dx.doi.org/10.1103/PhysRevB.79.115418

[12] A. Matulis and F.M. Peeters, Analogy between one-dimensional chain models and graphene, Am. J. Phys. **77**, 595 (2009), http://dx.doi.org/10.1119/1.3127143

[13] A. Matulis and G. Kiršanskas, Approximate description of decaying quasi-stationary state, Lith. J. Phys. **49**(4), 373–381 (2009), http://dx.doi.org/10.3952/lithjphys.49402

[14] A. Matulis and F.M. Peeters, Quasibound states of quantum dots in single and bilayer graphene, Phys. Rev. B **77**(11), 115423-1–7 (2008), http://dx.doi.org/10.1103/PhysRevB.77.115423

[15] V.V. Cheianov, V. Fal'ko, and B. Altshuler, The focusing of electron flow and a Veselago lens in graphene p-n junctions, Science **315**(5816), 1252–1255 (2007), http://dx.doi.org/

[16] J. Eroms, M. Zitzlsperger, D. Weiss, J.H. Smet, C. Albrecht, R. Fleischmann, M. Behet, J. De Boeck, and G. Borghs, Skipping orbits and enhanced resistivity in large-diameter InAs/GaSb antidot lattices, Phys. Rev. B **59**(12), R7829–R7832 (1999), http://dx.doi.org/10.1103/PhysRevB.59.R7829

[17] F.M. Peeters and A. Matulis, Quantum structures created by nonhomogeneous magnetic fields, Phys. Rev. B **48**(20), 15166–15174 (1993), http://dx.doi.org/10.1103/PhysRevB.48.15166

[18] M. Ramezani Masir, A. Matulis, and F.M. Peeters, Quasibound states of Schrödinger and Dirac electrons in a magnetic quantum dot, Phys. Rev. B **79**(15), 155451-1–8 (2009), http://dx.doi.org/10.1103/PhysRevB.79.155451